

Research Article: New Research | Cognition and Behavior

Defensive Behaviors Driven by a Hypothalamic-Ventral Midbrain Circuit

https://doi.org/10.1523/ENEURO.0156-19.2019

Cite as: eNeuro 2019; 10.1523/ENEURO.0156-19.2019

Received: 29 April 2019 Accepted: 17 June 2019

This Early Release article has been peer-reviewed and accepted, but has not been through the composition and copyediting processes. The final version may differ slightly in style or formatting and will contain links to any extended data.

Alerts: Sign up at www.eneuro.org/alerts to receive customized email alerts when the fully formatted version of this article is published.

Copyright © 2019 Mangieri et al.

This is an open-access article distributed under the terms of the Creative Commons Attribution 4.0 International license, which permits unrestricted use, distribution and reproduction in any medium provided that the original work is properly attributed.

Defensive Behaviors Driven by a Hypothalamic-Ventral Midbrain Circuit

Leandra R. Mangieri^{1,2}, Zhiying Jiang¹, Yungang Lu¹, Yuanzhong Xu¹, Ryan M. Cassidy^{1,2},
Nicholas Justice^{1,2}, Yong Xu⁴, Benjamin R Arenkiel⁵, and Qingchun Tong^{1,2,3,6}

6

7

1

2 3

¹ Brown Foundation Institute of Molecular Medicine of McGovern Medical School, University of

- 8 Texas Health Science Center at Houston, Houston, TX 77030, USA.² Graduate Program in
- 9 Neuroscience of MD Anderson Cancer Center UTHealth Graduate School of Biomedical
- 10 Sciences, University of Texas Health Science Center at Houston, Houston, TX 77030, USA.³
- 11 Department of Neurobiology and Anatomy of McGovern Medical School, University of Texas
- 12 Health Science Center at Houston, Houston, TX 77030, USA. ⁴Children's Nutrition Research
- 13 Center, Department of Pediatrics, Baylor College of Medicine. ⁵Department of Neuroscience,
- 14 Baylor College of Medicine, and Jan and Dan Duncan Neurological Research Institute, Texas
- 15 Children's Hospital.
- ¹⁶ ⁶Corresponding author: Qingchun Tong PhD, <u>Qingchun.tong@uth.tmc.edu</u>
- 17 Number of pages: 20
- 18 Number of Figures: 7; multimedia: 3 movie clips
- Word number in Abstract: 150; in Significance Statement: 98; in Abstract: 468 and inDiscussion: 1250
- 21 Acknowledgments: We would like to thank Dr. Zhengmei Mao for help with microscopy, and
- 22 Madhavi Jere for help with behavioral annotation. This study was supported by NIH R01
- 23 DK114279, R21NS108091 to QT; NIH 5F31DA041703 to LM; NIH R01DK117281,
- 24 R01DK101379 and P01DK113954 to Yong X; and R01DK109934 to B.R.A. and Q.T. We also
- acknowledge the Neuroconnectivity Core funded by NIH IDDRC grant 1 U54 HD083092 for
- 26 providing AAV vectors. QT is the holder of Cullen Chair in Molecular Medicine at McGovern
- Medical School. RC was supported by TL1 training grant 4TL1TR000369 (Center for Clinical and Translational Sciences, UTHealth). QT is the guarantor of this work and, as such, had full access to all the data in the study and takes responsibility for the integrity of the data and the
- 30 accuracy of the data analysis.
- 31 **Declaration of interests:** Authors declare no competing interests.
- 32

34 Abstract

33

The paraventricular hypothalamus (PVH) regulates stress, feeding behaviors and other 35 homeostatic processes, but whether PVH also drives defensive states remains unknown. Here 36 37 we showed that photostimulation of PVH neurons in mice elicited escape jumping, a typical 38 defensive behavior. We mapped PVH outputs that densely terminate in the ventral midbrain area, and found that activation of the PVH→ventral midbrain (vMB) circuit produced profound 39 40 defensive behavioral changes, including escape jumping, hiding, hyperlocomotion, and learned 41 aversion. Electrophysiological recordings showed excitatory post-synaptic input onto ventral midbrain neurons via PVH fiber activation, and in vivo studies demonstrated that glutamate 42 transmission from $PVH \rightarrow vMB$ was required for the evoked behavioral responses. 43 44 Photostimulation of PVH → vMB fibers induced cFos expression mainly in non-dopaminergic 45 neurons. Using a dual optogenetic-chemogenetic strategy, we further revealed that escape jumping and hiding were partially contributed by the activation of midbrain glutamatergic 46 47 neurons. Taken together, our work unveils a hypothalamic-vMB circuit that encodes defensive properties, which may be implicated in normal stress-induced defensive responses. 48 49 Keywords; PVH, midbrain, defense, glutamate, fear 50 51 52

52

53

54 Significance Statement

Paraventricular hypothalamus (PVH) neurons are known to be involved in various homeostatic 55 regulation. Despite the known activation of PVH neurons by various stresses, whether these 56 57 neurons are directly involved in defensive behaviors during stressful events is not clear. This 58 study reveals a direction projection from PVH to ventral midbrain (vMB) regions. Acute activation of either PVH neurons or specific PVH→vMB projections elicited stress, escape 59 jumping, hiding and learned aversion, all related to defensive behaviors, which was partially 60 contributed by midbrain glutamatergic neurons. Our study thus identifies a previously unknown 61 role for the PVH→vMB neural pathway in promoting a defensive behavioral program. 62 63

64

65 Introduction

Defensive behaviors encompass a repertoire of hard-wired responses critical for survival 66 in the animal kingdom (Blanchard and Blanchard, 2008). Perceived threats prompt expression 67 of fear, and result in escape behaviors, such as fleeing or freezing (Steimer, 2002). Such 68 behaviors are orchestrated by intricate neural networks, comprising multiple brain sites and 69 70 likely redundant pathways (Silva et al., 2016a). The hypothalamus is a complex structure that 71 contains spatially distinct groups of neurons with diverse functions. In addition to its well-72 established role in homeostatic processes via endocrine or autonomic control, the ventromedial 73 hypothalamus (VMH) is also implicated in innate defensive responses (Wang et al., 2015), as 74 well as the associated emotional states and learned responses to threat (Kunwar et al., 2015; 75 Silva et al., 2016b). Whether other hypothalamic neurons are also involved in innate behaviors is not clear. 76

77 The PVH has been classically described as a central hub for an array of autonomic and 78 neuroendocrine functions essential for homeostasis (Ferguson et al., 2008), and as a key output 79 node for adapting internal metabolic activity to energy status (Sutton et al., 2016). We have recently shown that the activity level of PVH neurons dictates feeding versus stress-related self-80 grooming, providing evidence that PVH may integrate information across several modalities to 81 82 adjust emotional and behavioral output (Mangieri et al., 2018). Indeed, recent studies suggest a 83 role for PVH neurons in mediating behavioral aspects of the stress response (Fuzesi et al., 84 2016). Given that encountering various stressors is an integral part of ensuing changes in emotional states and behavior, it is possible that PVH neurons are involved in these processes. 85 PVH neurons project to mesolimbic structures such as midbrain regions within and surrounding 86 87 the ventral tegmental area (VTA) (Geerling et al., 2010; Watabe-Uchida et al., 2012), and specific oxytocin projection to the VTA regulates pro-social behavior (Hung et al., 2017). Of 88 note, previous studies describe motivational and behavioral changes, including elicitation of 89 90 defensive behaviors, following electrical stimulation of broad PVH area (Atrens and Von, 1972; 91 Lammers et al., 1987; Lammers et al., 1988). However, whether PVH neurons directly drive 92 defensive behaviors is unknown. The VTA and nearby regions of the midbrain (thereafter referred to as ventral midbrain) are

The VTA and nearby regions of the midbrain (thereafter referred to as ventral midbrain) are composed of heterogeneous neuron populations, including dopaminergic, GABAergic and glutamatergic neurons (Morales and Margolis, 2017). Dopamine neurons are well known for driving reward, a positive emotional state, while glutamatergic neurons have recently been shown to drive aversion (Morales and Margolis, 2017), a negative emotion state associated with fear and anxiety. Here, we uncover a pathway from PVH to the ventral midbrain (vMB) region that drives innate defensive behaviors, including escape, learned avoidance, and feeding

- 100 suppression, some of which were partially mediated by midbrain glutamatergic neurons.
- 101 Collectively, these findings suggest that the PVH \rightarrow vMB projection represents a novel
- 102 component of defensive neurocircuitry, and provide a potential link between negative emotions
- 103 (stress and fear) and feeding abnormality.
- 104

105 Materials and Methods

106 Animals

Animal care and procedures were approved by the University of Texas Health Science Center 107 108 at Houston Institutional Animal Care and Use Committee. Mice were housed at 21-22°C on a 109 12 h light/ 12 h dark cycle (7 A.M. to 7 P.M. light), with ad libitum access to standard pellet chow, unless otherwise stated during fasting experiments. Sim1-Cre mice (Balthasar et al., 110 2005) were bred to Ai9 reporter mice (Madisen et al., 2010) to generate Sim1-Cre::Ai9; some 111 of the subjects used in behavioral experiments contained the reporter gene for post-hoc 112 visualization purposes. Sim1-Cre::Vglut2^{F/F} mice were generated as previously described (Xu 113 et al., 2013). Vglut2-ires-Cre mice (Vong et al., 2011) were purchased from Jackson Labs 114 115 (stock no. 016963) and bred to C57 mice to generate Vglut2-ires-Cre subjects used in the 116 experiments. Mice were at least 6 weeks old prior to surgeries and testing, and were chosen from multiple litters. All experiments were done in males during the light cycle, between the 117 early afternoon hours (12 P.M.) and early evening before the start of the dark cycle. 118

119

120 Viruses and Surgery

- 121 The following viral constructs were delivered to the PVH via stereotactic surgery:
- 122 For optogenetic experiments, AAV-EF1α-DIO-hChR2(H134R)-EYFP-WPRE-hGHpA serotype
- 123 2/9 (IDDRC Neuroconnectivity Core, Baylor College of Medicine, Houston, Texas); AAV-
- 124 EF1α-DIO-EGFP serotype DJ8 (IDDRC Neuroconnectivity Core, Baylor College of Medicine,
- 125 Houston, Texas); AAV-EF1α-DIO-iC++-EYFP (University of North Carolina Vector Core,
- 126 Chapel Hill, NC, USA);
- 127 For anterograde tracing, AAV-EF1α-FLEX-Syn-EGFP-WPRE-hGHpA, serotype DJ/8 (IDDRC
- 128 Neuroconnectivity Core, Baylor College of Medicine, Houston, Texas);
- 129 For ex vivo electrophysiological recordings of Vglut2 positive and negative neurons in the
- 130 midbrain, ChR2 virus as above was injected to PVH and AAV-EF1α-DIO-EGFP serotype DJ8
- 131 virus was injected to the midbrain to label Vglut2 positive cells;

For combined optogenetic/DREADD-mediated inhibition, ChR2 virus as above was injected
 to PVH and AAV1-EF1α-DIO-hM4D(Gi)-mCherry EYFP (University of North Carolina Vector

134 Core, Chapel Hill, NC, USA) was injected in the midbrain-VTA area.

For fiber photometry experiments, AAV-EF1α-FLEX-GCaMP6m (IDDRC Neuroconnectivity
 Core, Baylor College of Medicine, Houston, Texas) was delivered to the midbrain-VTA area.
 All viral preparations were tittered to at least 10¹¹ particles/mL.

Stereotaxic surgeries to deliver viral constructs and for optical fiber implantation were 138 139 performed as previously described (Mangieri et al., 2018). Briefly, mice were anesthetized with a ketamine/xylazine cocktail (100 mg/kg and 10 mg/kg, respectively), and their heads 140 141 affixed to a stereotaxic apparatus. Viral vectors were delivered through a 0.5 µL syringe 142 (Neuros Model 7000.5 KH, point style 3; Hamilton, Reno, NV, USA) mounted on a motorized stereotaxic injector (Quintessential Stereotaxic Injector; Stoelting, Wood Dale, IL, USA) at a 143 rate of 40 nL/min. Viral delivery was targeted to the PVH (100 nL/side; AP: −0.5 mm; ML:±0.2 144 145 mm; DV: -5.0 mm) or midbrain/VTA area (200-300 nL/side AP: -2.4 mm; ML:±0.5 mm; DV: 146 -4.6 mm). Uncleaved fiber optic cannulae (Ø1.25 mm Stainless Ferrule, Ø200 µm Core, 0.39 NA; ThorLabs, Newton, New Jersey, USA) were precut to 4.5-4.8 mm and implanted above 147 the PVH (AP: -0.5 mm; ML: 0 mm) or precut to 4.3-4.5 mm and implanted above 148 149 midbrain/VTA (AP: -2.4 mm; ML: +0.5 mm). For glutamate receptor blockade experiments, a single cannula system allowing for interchangeable optic fiber and fluid delivery (Plastics1, 150 151 Roanoke, VA) was implanted above the midbrain/VTA area. For fiber photometry, uncleaved fiber optic cannulae (Ø1.25 mm Stainless Ferrule, Ø400 µm Core, 0.39 NA; ThorLabs, 152 153 Newton, New Jersey, USA) were precut to 4.3-4.5 mm and implanted above the midbrain/VTA area. All cannulae implants were secured on the head with adhesive gel 154 (Loctite 454) and dental cement. Experiments were conducted on subjects after a 3-4 week 155 recovery period following surgery. 156

157

158 Acute Brain Slices Preparation and *in vitro* Electrophysiology Recordings.

For Sim1-Cre mouse recordings, coronal brain slices (250–300 μm) containing the PVH or
VTA from mice that had received stereotaxic injections of AAV-FLEX-ChR2-EYFP to PVH at
least 3 weeks prior to the recording were cut in ice-cold artificial cerebrospinal fluid (aCSF)
containing the following (in mM): 125 NaCl, 2.5 KCl, 1 MgCl₂, 2 CaCl₂, 1.25 NaH₂PO₄, 25
NaHCO₃, and 11 D-glucose bubbling with 95% O₂/5% CO₂. Slices containing the PVH were
immediately transferred to a holding chamber and submerged in oxygenated aCSF. Slices
were maintained for recovery for at least 1 h at 32–34 °C before transferring to a recording

166 chamber. Individual slices were transferred to a recording chamber mounted on an upright microscope (Olympus BX51WI) and continuously superfused (2 ml/min) with ACSF warmed 167 to 32-34 °C by passing it through a feedback-controlled in-line heater (TC-324B; Warner 168 169 Instruments). Cells were visualized through a 40X water-immersion objective with differential interference contrast (DIC) optics and infrared illumination. Whole cell current-clamp 170 recordings were made from neurons within the regions of the PVH showing high density of 171 ChR2-EYFP expression, and whole cell voltage-clamp recordings in VTA/midbrain region 172 173 were performed on cells surrounded by dense ChR2-EYFP expressing fibers. Pipettes were 174 filled with a K⁺-based low Cl⁻ internal solution containing (in mM) 145 KGlu, 10 HEPES, 0.2 175 EGTA, 1 MgCl₂,4 Mg-ATP, 0.3 Na₂-GTP, 10 Na₂-Phosphocreatine (pH 7.3 adjusted with 176 KOH; 295 mOsm) for current clamp recordings. For voltage-clamp recordings, Patch pipettes (3–5 M Ω) were filled with a Cs⁺-based low Cl⁻ internal solution containing (in mM) 135 177 CsMeSO₃, 10 HEPES, 1 EGTA, 3.3 QX-314, 4 Mg-ATP, 0.3 Na₂-GTP, 8 Na₂-178 179 Phosphocreatine (pH 7.3 adjusted with CsOH; 295 mOsm). Membrane potentials were corrected for ~10 mV liquid junction potential. To activate ChR2-expressing neurons in PVH 180 or CHR2-fibers in VTA/midbrain, light from a 473 nm laser (Opto Engine LLC, Midvale, UT, 181 USA) was focused on the area of the recorded PVH neuron to produce spot illumination 182 183 through optic fiber. Brief pulses of light (blue light, 1-2 ms, 1-2 mW/mm²) were delivered at the recording site at 10–15 s intervals under control of the acquisition software. 184 185 Vglut2-ires-cre mice, at least 3 weeks following virus infection, were anesthetized and brains were obtained for recording. Horizontal slices (250 µm) containing the VTA were 186 187 sectioned using a Leica VT 1000S vibratome, and transferred to a holding chamber with artificial cerebrospinal fluid (aCSF) containing (in mM): 123 NaCl, 26 NaHCO₃, 2.5 KCl, 1.25 NaH₂PO₄, 188 10 glucose, 1.3 MgCl₂, and 2.5 CaCl₂, and saturated with 95% O₂/5% CO₂ at 32°C for 1h, then 189 maintained at room temperature to allow for recovery prior to any electrophysiological 190 191 recordings. Individual slices were transferred from the holding chamber to a heated recording 192 chamber (31-33°C, Luigs-Neumann), in which they were submerged and continuously perfused 193 with oxygenated aCSF at a rate of 2-3ml/min. Recordings were performed under infrareddifferential interference contrast visualization on a fixed stage, upright microscope (Olympus 194 BX51WI) equipped with a water immersion 40x objective. Pipettes with resistance 3-5 M Ω were 195 196 pulled from borosilicate glass (OD 1.5 mm, ID 1.1 mm, Sutter Instruments) using a horizontal 197 puller (Sutter P-1000), and filled with an internal patch solution containing (in mM): 142 K-

198 gluconate, 10 HEPES, 1 EGTA, 2.5 MgCl₂, 0.25 CaCl₂, 4 Mg-ATP, 0.3 Na-GTP, and 10 Na₂-

199 phosphocreatine, adjusted to pH 7.25-7.35, osmolality 295-305 with KOH. Whole-cell patch-

clamp recordings data were digitized and collected using Multiclamp 700B amplifier, and
Digidata 1550B digitizer, and Clampex 10 (Molecular Devices). Membrane potential was held at
-60mV. The liquid junction potential was not corrected, and series resistance (Rs) was bridge
balanced. Offline data analysis was performed using Clampfit 10 (Molecular Devices). To excite
channelrhodopsin in brain slices, we illuminated the brain slices every 30s with blue light pulses
(473 nm PSU-III-LED laser system, Optoengine), of short duration (1-3ms) through 40x waterimmersion objective lens.

207 Optogenetic Experimental Parameters

For in vivo photostimulation/inhibition, an integrated rotary joint patch cable connected the 208 ferrule end of optic fiber cannula with a Ø1.25 mm ferrule end of the patch cable via a mating 209 210 ceramic sleeve (ThorLabs, Newton, New Jersey, USA). At the other end of the rotary joint, an 211 FC/PC connector was connected to a 473 nm diode-pumped solid state (DPSS) laser (Opto Engine LLC, Midvale, Utah, USA). Light pulses were controlled by Master-8 pulse stimulator 212 213 (A.M.P.I., Jerusalem, Israel). For behavioral experiments requiring a large chamber (Real 214 Time Place Preference/Avoidance, locomotion, and escape hut assays) a commutator (rotary 215 joint; Doric, Québec, Canada) was attached to a patch cable via FC/PC adapter. The patch cable was then attached to the optic fiber cannula ferrule end via a ceramic mating sleeve. 216 217 Another patch cable containing FC/PC connections at both ends allowed the connection 218 between the commutator and the laser, which was controlled by the Master-8 pulse 219 stimulator. During testing, mice were placed in a clean, high-walled enclosure or in a large 220 chamber wiped down with 70% isopropyl alcohol. Light power was measured before starting 221 experiments each day with an optical power meter (ThorLabs), and adjusted to emit an output of 5-15 mW from the end of the mating sleeve. 222

223

224 Behavioral Analysis

225 Grooming and Escape Jumping. To measure the effects of photostimulation on the baseline behavior, mice were placed in a clean, high-walled enclosure, which prevented escape from 226 227 the chamber. Sim1-Cre mice were observed for grooming and recorded with a hand-held 228 camera for a 15 minute period with the following protocol: 5 minutes, no light (Pre), 5 minutes, light-on (On), and 5 minutes post-light (Post). A 6 minute observation period for 229 jumping behavior in Sim1-Cre mice was performed following 2 minutes pre-light, 2 minutes 230 231 light-on, and 2 minutes post-light. Vglut2-ires-cre mice were observed similarly for grooming 232 and jumping during the 15 minute protocol.

233 For PVH photostimulation, light was pulsed at a 5 Hz frequency with 10 or 100 ms pulse duration, and 20 Hz, 10 ms for PVH \rightarrow vMB photostimulation. Behavioral changes were 234 annotated by watching the videos using QuickTime Player (Apple). Time spent grooming 235 was carefully annotated by noting the video timestamps at the beginning and end of 236 grooming bouts. Beginning of bouts was defined as the moment the animal started engaging 237 238 in forelimb paw strokes made near the nose, eyes, and head, and licking of paw, body, tail, 239 or genitals, and the end of bouts was noted when grooming was interrupted for at least 6 240 seconds. The latency to start grooming was defined as the precise time mice started grooming following the first pulse of light. Number of jumps during the 15 minute test was 241 242 quantified by watching videos in slow motion and counting each jump mice made, as defined 243 by removal of limbs from the floor of the cage and complete suspension of the body in air. Grooming and escape jumping observations were also performed one hour following 244 intraperitoneal (i.p.) injection of saline or CNO (1 mg/kg) in Vglut2-ires-Cre mice expressing 245 246 hM4D(Gi)-mCherry in the vMB.

247

260

248 Glutamate Receptor Blockade. Mice implanted with interchangeable fluid delivery/optic fiber cannula system (Plastics1, Roanoke, VA) were anesthetized with isoflurane and placed in a 249 250 stereotactic apparatus. A microinjection volume of 100 nL, directed to the midbrain/VTA 251 area, was slowly infused at an approximate rate of 33 nL/min. Three minutes following 252 infusion, fluid delivery cannula were removed from the guiding cannula and replaced with 253 optic fiber cannula, and mice were allowed to recover from anesthesia for 10-15 minutes 254 prior to testing. Mice were then placed in a high-walled enclosure and video recorded for 5 255 minutes during photostimulation (20 Hz, 10 ms pulses). Jumping behavior was annotated as described above. Two separate trials were performed at the same mice on separate days: a 256 257 control (vehicle injection) trial and drug (glutamate receptor blockade injection) trial. Vehicle 258 injections consisted of 15% DMSO, while drug injections consisted of 300 ng D-AP5 + 150 ng 259 DNQX (Tocris, Minneapolis, MN) suspended in 15% DMSO.

Locomotion. Mice were placed in a large (45 X 45 X 50 cm³) chamber, equipped with an
 overhead infrared camera (PhenoTyper system 3.0, Noldus, Wageningen, the Netherlands),
 and allowed to freely roam during a 15 minute test, consisting of 5 minutes no-light, 5
 minutes light-on, and 5 minutes post-light. Light was pulsed at 5 Hz, 10 ms for PVH
 photostimulation, and 20 Hz, 10 ms for PVH → vMB photostimulation. Locomotion assays
 were also performed one hour following intraperitoneal (i.p.) injection of saline or CNO (1

mg/kg) in Vglut2-ires-Cre mice expressing hM4D(Gi)-mCherry in the vMB. Locomotion data,
including total distance travelled and average velocity, were collected by tracking software
(EthoVision XT 11.5, Noldus) for each 5 minute period. Activity tracks were visualized by
plotting movement of the mouse based on center point location, as captured by the overhead
camera.

272

273 Real Time Place Preference/Avoidance Assays. For RTPP/A assays, mice were allowed to freely explore a large 45 X 45 X 50 cm³ chamber, as detailed above, during a 20 minute 274 testing period. The chamber was evenly divided into two sectors, one of which was randomly 275 276 assigned as the light-on side. Crossing over and occupying the light-paired side of the 277 chamber triggered continuous pulsing of light (5 Hz, 100 ms light pulses for PVH photostimulation, and 20 Hz, 10 ms pulses for PVH \rightarrow vMB photostimulation), which ceased 278 279 once animals returned to the light-off side. The side of the chamber paired with light was 280 counterbalanced during experiments for each mouse. RTPP/A assays were performed one 281 hour following intraperitoneal (i.p.) injection of saline or CNO (1 mg/kg) in Vglut2-ires-Cre mice expressing hM4D(Gi)-mCherry in the midbrain. The percent time spent on each side 282 and time spent in the food zone, as well as the tracking data, were collected by EthoVision 283 284 tracking software (Noldus). Heatmaps detailing proportion of time spent in each location of 285 the arena, as well as activity tracks, were visualized based on the data collected. 286

287 Modified RTPP/A Assay-Fast Refeed. Mice were fasted 24h prior to testing fast-refeeding in 288 a large chamber containing food in one corner of the arena. The location of food was rotated 289 amongst four corners of the cage, and the light-paired side was counterbalanced for each mouse tested. Upon crossing into the light-paired side, light was pulsed through the optical 290 291 fiber into the brain at 5 Hz, 10 ms for PVH activation or 20 Hz, 10 ms for PVH→vMB 292 activation, and ceased upon exit into the light-unpaired side. Total testing time lasted 15 293 minutes. The percent time spent on each side and time spent in the food zone, as well as 294 the tracking data, were collected by EthoVision tracking software (Noldus). Heatmaps detailing proportion of time spent in each location of the arena, as well as activity tracks, 295 296 were visualized based on the data collected.

297

Conditioning Assay. Sim1-Cre mice with ChR2 injected into the PVH and optical fibers placed
 over the ventral midbrain, were placed in a large testing chamber with flooring on one side
 lined with several columns of green tape spanning the top to bottom edges of the cage. On

301 day 0, mice tethered to an optic fiber cable delivering no light, were allowed to freely explore 302 the arena for 20 minutes; the side most preferred, as determined by percent time spent on 303 each side, was noted and assigned as the light-paired side for the subsequent days of 304 conditioning. For the next 4 days of conditioning, mice were tested approximately at the 305 same time for 20 minutes, during which optic fiber cable delivered 20 Hz, 10 ms photostimulation upon crossing the light-paired side of the chamber, and ceased once mice 306 307 traversed to the light-off side. Mice were thereafter tested for 20 minutes on days 5-6 for 308 extinction, during which light was no longer delivered through the optic fiber. The preference for the light-on zone, initially the most preferred side, was calculated as the percent time 309 310 mice spent in the light-paired side of the chamber for each trial. Locomotion data to calculate the distance travelled during testing sessions were collected by EthoVision tracking software 311 312 (Noldus).

313

314 Escape Hut Assay. For this assay, an "escape hut", equipped with a single entry and three 9.5 cm walls with no "roof" (in order to maintain top-down visualization of tracking from the 315 316 overhead camera) was placed in the center of a large chamber. Testing was performed one 317 hour following intraperitoneal (i.p.) injection of saline or CNO (1 mg/kg) in Vglut2-ires-Cre 318 mice expressing hM4D(Gi)-mCherry in ventral midbrain. Mice were first acclimated to the 319 novel environment for seven minutes, which allowed sufficient time for spontaneous 320 discovery of the hut. After acclimation, an eight-minute testing period immediately followed, 321 in which light was continuously pulsed at 5-10 Hz (10 ms pulse width) every other minute. 322 The number of hut visits (defined as the number of times the animal approached and entered 323 the hut) and duration in the hut (quantified as the time spent inside the hut enclosure) were quantified by EthoVision software (Noldus). Number of hut visits and total time spent inside 324 325 the hut across each time interval (Off vs. On) was combined for statistical analysis. Total 326 distance travelled during each time interval was also combined for analysis, and velocity was 327 averaged across each light-off and light-on periods to reveal average velocity during the two 328 light conditions. Heatmaps across time intervals were constructed based on tracking data collected by EthoVision software. 329

330

331 Immunohistochemistry and Imaging

- 332 After behavioral experiments were completed, study subjects were anesthetized with a
- 333 ketamine/xylazine cocktail (100 mg/kg and 10 mg/kg, respectively) and subjected to
- transcardial perfusion. Freshly fixed brains were then extracted and placed in 10% buffered

335 formalin at 4 °C overnight for post-fixation. The next day, brains were transferred to 30% sucrose solution and allowed to rock at room temperature for 24 h prior to sectioning. Brains 336 were frozen and sectioned into 30 µm slices with a sliding microtome and mounted onto 337 slides for post-hoc visualization of injection sites and cannula placements. Injection sites 338 were determined by the densest regions of EYFP, EGFP, or mCherry fusion products. The 339 location of cannula implants were noted by prominent lesion sites that extended over the 340 341 rostro-caudal axis of the PVH or the ventral midbrain area. Mice with missed injections to the 342 PVH or ventral midbrain, or those with misplaced optic fibers over the areas of interest were excluded from behavioral analysis. Representative pictures of PVH, PVH projections, and 343 344 ventral midbrain injection sites were visualized with confocal microscopy (Leica TCS SP5; Leica Microsystems, Wetzlar, Germany). Brain sections used for immunohistochemistry 345 (IHC) were stained with the following primary antibodies, followed by secondary antibodies: 346 mouse anti-tyrosine hydroxylase (TH) (Millipore, MAB318)/Alexa Fluor 488, donkey anti-347 348 mouse or Alexa Fluor 594 donkey anti-mouse; rabbit anti-cFos (Cell Signal #2250)/Alexa 349 Fluor 488 donkey anti-rabbit or Alexa Fluor 594 donkey anti-rabbit. Sim1-Cre mice used for cFos analysis were placed separately in clean testing cages, provided with food, water, and 350 351 bedding for two hours prior to photostimulation. Mice were then photostimulated with 20 Hz 352 light pulses (10 ms pulse duration) for five seconds, followed by five seconds of no light, 353 repeated for 15 minutes. Following photostimulation, mice were subjected to transcardial 354 perfusion 1.5 hours later and brain sections were processed for IHC. Vglut2-ires-Cre mice used for cFos analysis were first i.p. injected with CNO, and placed in clean testing cages 30 355 356 minutes prior to photostimulation. Photostimulation was then applied for 15 minutes (20 Hz. 10 ms pulses every five seconds), and mice were transcardially perfused 1.5 hours later. 357

359 Statistics

358

GraphPad Prism 7 software (La Jolla, CA) was used for statistical analysis. Two-way repeated
measures ANOVA, followed by Dunnett's or Sidak's multiple comparisons tests, and ordinary or
repeated measures one-way ANOVA tests, followed by Dunnett's or Tukey's multiple
comparisons test, were used for comparisons of more than two groups. Paired or unpaired twotailed t-tests were used for comparing two groups. Pearson correlation (two-tailed) was used to
analyze correlation between two variables. Data in figures, text and legends were expressed as
means ± SEMs. Significance levels were denoted by asterisks: *p<0.05, **p<0.01, ***p<0.001.

368 Results

Activation of PVH neurons elicits escape behavior associated with increased flight and negative valence

Through targeted manipulation of PVH neurons, we recently uncovered a novel 371 372 hypothalamic site that bidirectionally controls feeding and repetitive, stress-like self-grooming (Mangieri et al., 2018). Here, we aimed to explore and characterize other behavioral responses 373 374 by manipulating PVH neural activity. To this end, we injected cre-dependent channelrhodopsin-375 2 (ChR2) expression viral constructs into the PVH of Sim1-Cre mice (Sim1-Cre::ChR2^{PVH}), 376 allowing optogenetic manipulation of the majority of PVH neurons (Balthasar et al., 2005) (Fig. 377 1A). Photostimulaton with long pulses of blue light (100 ms) at 5 Hz reliably elicited time-locked 378 activation of PVH neurons (Fig.1B). Similar to our previous findings, in vivo photostimulation of PVH neurons at 5Hz-100ms produced repetitive self-grooming in the majority of ChR2-379 expressing mice (Fig.1C). The same photostimulation in Sim1-Cre::ChR2^{PVH}::Vglut2^{F/F} mice 380 (also known as knockouts, KOs), which lacked vesicular glutamate transporter 2 (Vglut2, 381 382 required for presynaptic glutamate release) in Sim1-neurons, also showed a robust increase in repetitive grooming time during light-on periods that was not significantly different than that seen 383 in Sim1-Cre::ChR2^{PVH} mice (Fig.1C). However, self-grooming in Sim1-Cre::ChR2^{PVH} mice was 384 more fragmented than in KO mice (Movie S1 and S2). Notably, latency to initiate grooming after 385 386 light illumination was significantly longer in KOs (Fig. 1D and Movie S2). We also noted a trend towards fewer grooming bouts in KOs (Figs. 1E-1F). These results suggest that glutamate 387 388 release, although not absolutely required for, contributes significantly to the light-induced selfgrooming. Interestingly, however, we noted that both 5Hz-10ms (Fig. 1G) and 5 Hz-100 ms (Fig. 389 1H) photostimulation elicited frantic escape-like jumping in the majority of Sim1-Cre::ChR2^{PVH} 390 mice (Movie S3), but not in KOs (Figs. 1G and 1H). Notably, the shorter pulse duration (10ms, 391 5Hz) elicited less jumping responses in Sim1-Cre::ChR2^{PVH} mice tested, and jumping behavior 392 increased in response to the longer length of light-pulses (Fig. 11), indicating scalability of the 393 behavior via strength of neural activation. We also observed that some Sim1-Cre::ChR2PVH 394 395 mice displayed only grooming or jumping to the exclusion of the other, while others showed a 396 mix of behaviors during the photostimulation session. In fact, we noted a negative correlation between the two behaviors (Fig. 1J), consistent with the mutually exclusive nature of such 397 behaviors. Thus, the self-grooming behavior elicited by photostimulation in Sim1-Cre::ChR2^{PVH} 398 399 mice (Fig. 1C) might be underestimated due to conflicting jumping behaviors (Fig. 1G). No selfgrooming (Fig. 1K) or jumping (Fig. 1L) was observed in GFP-injected controls (Sim1-400 Cre::GFP^{PVH}), suggesting a specific effect of photostimulating PVH neurons in promoting the 401 402 behaviors.

We also found that photostimulation in Sim1-Cre::ChR2^{PVH} mice dramatically increased 403 404 overall locomotion compared to controls (Fig. 2A), affecting both total distance travelled (Fig. 2B) and average velocity (Fig. 2C), suggesting an elevated state of arousal and agitation. We 405 next probed the emotional valence of PVH activation using a real-time place 406 preference/avoidance assay (RTPP/A) (Jennings et al., 2013b). Compared to GFP controls, 407 Sim1-Cre::ChR2^{PVH} mice avoided the light-paired side of the testing chamber, though total 408 distance travelled was unchanged (Figs. 2D-2F). As an additional comparison, we tested the 409 valence of inhibiting PVH neurons in the RTPP/A assay by using Sim1-Cre mice injected with 410 cre-dependent inhibitory opsin, iC++ (Sim1-Cre::iC++^{PVH}) (Berndt et al., 2016; Mangieri et al., 411 412 2018). Surprisingly, inhibition of PVH neurons did not elicit significant preference or avoidance 413 to the light-paired side (Figs. 2D-2F), which was previously shown to promote feeding and reduce stress-induced grooming (Mangieri et al., 2018). Collectively, these results indicate that 414 glutamate release from PVH neurons drives a scalable increase in escape behavior, while both 415 416 glutamate and non-glutamate action contribute to self-grooming. 417 418

PVH projections to the midbrain area drive escape behavior and avoidance

419 To probe potential PVH targets for the observed behaviors, we injected cre-dependent, 420 synaptophysin constructs (AAV-FLEX-Syn-EGFP) to PVH neurons of Sim1-Cre mice for anterograde tracing (Herman et al., 2016) (Figs. 3A-2B). We observed dense projections in 421 422 previously reported sites, such as the median eminence (ME), periaqueductal gray (PAG)/dorsal raphe (DR), parabrachial nucleus (PBN), and locus coeruleus (LC) (data not shown). 423 424 Interestingly, we observed substantial puncta in the midbrain area, both within and surrounding 425 the VTA, most notably in the area medial to VTA and above the mammillary nucleus (supramammillary nucleus, SUM) and caudally into the VTA area (thereafter called midbrain) 426 (Figs. 3C-3E). To evaluate functional connectivity, we photostimulated local Sim1-Cre::ChR2PVH 427 428 fibers in the midbrain (Fig. 3F), which evoked time-locked, excitatory post-synaptic currents in 429 midbrain neurons in 8 out of 15 midbrain neurons recorded, indicating glutamatergic transmission. Following PVH→midbrain photostimulation, we found that compared to GFP 430 controls (Sim1-Cre::GFP^{PVH->vMB}) mice (Fig. 3G, left panels), Sim1-Cre::ChR2^{PVH->vMB} mice (Fig. 431 3G, right panels) had a greater number of cFos-labeled neurons in ventral midbrain and SUM 432 433 (Fig. 3H). Most cFos expression was found in the area of the anterior midbrain and medial to the VTA. Notably, few cFos-labeled cells were detected in the VTA region proper, and within the 434 area with a comparable TH+ neurons, cFos was found in very few TH+ cells (Fig. 3I), consistent 435

with tracing results showing a substantial portion of PVH projections terminating in the SUM andthe area medial to the VTA.

Empirically, we found that 20 Hz-10ms photostimulation of the PVH -> midbrain circuit in live 438 Sim1-Cre::ChR2 PVH->vMB animals resulted in the most obvious behavioral changes, including 439 increased grooming behavior post-stimulation (Fig. 4B), and escape-jumping similar to that seen 440 with PVH photostimulation (Fig. 4D). The same photostimulation failed to enact obvious 441 repetitive grooming or escape jumping in GFP controls (Figs. 4A and 4C). In contrast, Sim1-442 Cre::ChR2 PVH->vMB::Valut2^{F/F} (KO) mice exhibited a significant increase in grooming during and 443 after the photostimulation period, but showed no jumping behavior (Figs. 4B and 4D). Of note, 444 the effect on self-grooming behavior in Sim1-Cre::ChR2 PVH->VMB mice might be underestimated 445 owing to competing jumping behavior. We found that microinfused glutamate receptor 446 antagonists to ventral midbrain of Sim1-Cre::ChR2 PVH->vMB mice prior to photostimulation 447 significantly reduced the escape jumping in response to photostimulation (Figs. 4E and 4F), 448 449 confirming that ventral midbrain neurons mediate the behavior. Similar to PVH activation, we also noted that photostimulation of PVH fibers in ventral midbrain promoted locomotor activity in 450 Sim1-Cre::ChR2 PVH->vMB mice (Figs. 4G and 4H), but not in GFP controls (Figs. 4G and 4H) or 451 KO mice (data not shown), suggesting an essential role for glutamate release in promoting 452 453 locomotor activity.

Interestingly, we found that place avoidance caused by PVH→vMB photostimulation in the RTPP/A assay required glutamatergic transmission (Figs. 4I and 4J), but did not affect the total distance travelled during the assay (data not shown). These results suggest that glutamatergic transmission from PVH→vMB promotes a state of negative valence, coupled by a drive for flight and escape.

459

Activation of PVH→ventral midbrain circuit suppresses food intake and promotes aversion learning

462 We previously demonstrated that photostimulation of PVH neurons abruptly halts ongoing 463 feeding, and in turn promotes repetitive grooming, a phenomenon that was reversible upon light termination (Mangieri et al., 2018). To examine whether place avoidance elicited by PVH 464 neuron activation would alter feeding, we modified the RTPP/A assay by placing food in a 465 466 corner of the light-paired side of the arena (Fig. 5A). Following 24-h fast, GFP control mice 467 approached the light-paired side of the chamber and proceeded to consume the food (Fig. 5B, 5C-5D). In contrast, ChR2 mice attempted to approach the food zone, but spent significantly 468 less time in the light-on side and food zone (Figs. 5B right panel, 5C-5D), and consequently ate 469

470 significantly less than controls (Fig. 5E). Given that total locomotion during the assay was 471 unchanged between groups, together these data suggest that negative valence triggered by PVH photostimulation was sufficient to repel mice from an extremely salient goal, i.e., re-feeding 472 after a long fast. We next performed the same assay on mice with photostimulation of local 473 PVH fibers in ventral midbrain, and similarly found that Sim1-Cre::ChR1^{PVH->vMB} mice spent 474 significantly less time in the light-paired side and food zone (Fig. 5F-5H), and consumed 475 476 significantly less (Fig. 5I). On the other hand, upon locating food, KO mice with the same 477 stimulation tended to remain in the light-paired side (Fig. 5F), and spent a similar amount of time in the light-on side and food zone as GFP controls (Fig. 5G-5H). The food intake in KO mice 478 479 was more than that in the ChR2 group, but significantly less than GFP controls (Fig. 5I). The total distance travelled during the assay was unchanged between GFP control and Sim1-480 Cre::ChR1^{PVH->vMB} mice, but was significantly reduced in KO mice (data not shown). These data 481 suggest a role for both glutamatergic and non-glutamatergic transmission in mediating the 482 483 $PVH \rightarrow vMB$ circuit on feeding and locomotion during the fasted state.

Given the known role for the midbrain in learning, we next tested whether the aversion 484 associated with light stimulation of PVH→midbrain could be learned. Sim1-Cre::ChR1^{PVH->vMB} 485 and GFP control mice were conditioned across several consecutive days by pairing a previously 486 preferred side of a chamber with light stimulation (Fig. 5J). As expected, Sim1-Cre::ChR1^{PVH-} 487 >vMB mice avoided the light-paired side during the four days of conditioning, spending 488 significantly less time in that side (Fig. 5K). Interestingly, Sim1-Cre::ChR1^{PVH->vMB} mice 489 persisted in avoiding the light-paired side during 24-h and 48-h extinction tests, when light was 490 491 no longer applied (Fig. 5K). Day-to-day changes in locomotion during the entire testing session was unchanged between groups (Fig. 5L). Thus, the PVH→vMB circuit promotes a learned 492 493 aversion process.

494

Glutamatergic midbrain neurons are activated by PVH projections to drive escape behavior

Previous studies reported that glutamatergic neurons in vMB respond to aversive cues (Root et al., 2018), and their projections to the nucleus accumbens and lateral habenula drive aversion (Root et al., 2014; Qi et al., 2016). Since these glutamatergic neurons are located in the same region that receives dense PVH projections, i.e. the area medial to the VTA, we wonder whether PVH projections target glutamatergic neurons in the midbrain to promote aversion and escape behaviors. Since Sim1-Cre co-localizes with the majority of Vglut2 neurons in the PVH (Xu et al., 2013), we used the Vglut2-ires-Cre mouse model (Vong et al., 504 2011) to target PVH neurons. To determine circuit connectivity, we delivered AAV-FLEX-ChR2-505 EYFP viruses to the PVH, and AAV-FLEX-GFP to vMB to visualize glutamatergic neurons. We 506 performed whole-cell recordings on glutamatergic neurons in vMB, while photostimulating local PVH-Vglut2 fibers expressing ChR2 (Fig. 6A). We found that all GFP+ neurons patched 507 showed excitatory post-synaptic currents (oEPSCs) (Fig. 6B). The currents could be blocked by 508 509 bath application of tetrodotoxin (TTX), and subsequently rescued by 4-aminopyridine (4-AP), suggesting monosynaptic connectivity (Fig. 6C). We noted that the majority of GFP- cells 510 511 patched (18/20) also received monosynaptic excitatory input from PVH (Fig. 6D), with a comparable latency and amplitude to GFP+ cells (Fig. 6E), suggesting diffusive innervation of 512 513 PVH fibers onto midbrain neurons. To examine the function of glutamatergic midbrain neurons, we silenced them prior to photostimulation by administrating clozapine-n-oxide (CNO) in Vglut2-514 ires-Cre mice injected with AAV-FLEX-hM4D(Gi)-mCherry virus into vMB and AAV-FLEX-ChR2-515 EYFP into the PVH (Figures 4F-G). Photostimlation of PVH \rightarrow vMB fibers produced cFos 516 517 expression in vMB, many of which were found in glutamatergic neurons (Fig. 6H, top panels). Injection of CNO prior to PVH→midbrain photostimulation reduced cFos expression in vMB (Fig. 518 6H, bottom panels), suggesting effective CNO-induced inhibition of vMB glutamatergic neurons. 519 Behaviorally, CNO administration in Vglut2-ires-Cre mice injected with AAV-FLEX-520 521 hM4D(Gi)-mCherry virus into vMB and AAV-FLEX-ChR2-EYFP into the PVH failed to affect self-522 grooming behavior (Fig. 7A), place avoidance (data not shown), or increased locomotion (data 523 not shown) evoked by photostimulating the $PVH \rightarrow vMB$ circuit. However, CNO significantly 524 reduced light-evoked escape jumping (Fig. 7B), indicating that vMB glutamatergic neurons play 525 a significant role in escape, but not in other defensive behaviors evoked by light stimulation. A recent study showed that mice consistently and predictably return to a previously memorized 526 shelter location upon experiencing threatening stimuli (Vale et al., 2017), so we next sought 527 528 to explore the function of vMB glutamatergic neurons in this type of escape strategy. 529 Towards this, we first injected Vglut2-ires-Cre mice with dual viral constructs as above, and 530 then placed them in a testing chamber containing a shelter ("escape hut") located in the middle 531 of the arena (Fig. 7C). Mice were acclimated to the testing environment for 7 minutes to allow spontaneous discovery of the shelter (Vale et al., 2017), then were exposed to 1 minute periods 532 of no light, followed by 1 minute intervals of light-on, repeated for eight minutes (Fig. 7C). Light 533 534 was pulsed at a lower frequency (5 Hz, 10ms) during light-on periods to preclude potential 535 interference from jumping activity. Remarkably, mice injected with saline prior to the trial 536 consistently approached and hid in the shelter during the light-on epochs (Fig.7D, top panels; Fig. 7F). In contrast, although most mice injected with CNO approached the shelter during light-537

16

on periods (Fig. 7E)) and displayed similar increases in locomotion upon light stimulation during
the assay (data not shown), they spent significantly less time hiding in the shelter (Fig. 7D,
bottom panels; Fig. 7F). These findings provide further evidence that PVH projections onto
midbrain glutamatergic neurons drive escape behaviors.

543 Discussion

542

544 Threatening stimuli prompt a state of fear, leading to various defensive behavioral 545 strategies, such as flight, avoidance, freezing, risk assessment and learned aversion, and compete with ongoing activities to promote survival (Blanchard and Blanchard, 2008). In this 546 547 study, we describe a hypothalamic-vMB circuit engaged in triggering a classic set of emotional and behavioral aspects typical of defense. Notably, we found that the PVH \rightarrow vMB connection 548 drives acute and learned aversion, and is capable of increasing locomotion, and escape 549 behaviors. The aversive properties of PVH \rightarrow vMB activation can override intrinsic homeostatic 550 551 drive for feeding. From these results, we propose that the PVH→vMB circuit is part of the neural 552 circuitry underlying behavioral and emotional processes that facilitate survival in a threatening situation. 553

We and others have previously shown that PVH neurons and specific neural subsets 554 555 constitute a critical node for evoking idiosyncratic behaviors, such as self-grooming, following stress (Fuzesi et al., 2016; Mangieri et al., 2018). Our data here support the idea that the PVH 556 557 signals negative valence, and is sufficient to produce stress-like and defensive responses. Given that repeated encounters with stressful situations may lead to a state of fear and 558 559 avoidance (Steimer, 2002), it is not surprising that the same neural populations transmit interrelated messages. Although the hypothalamus has been previously regarded as a relay 560 station for unconditioned defensive behaviors (Canteras, 2008), our study and others (Jennings 561 562 et al., 2013a; Sternson, 2013; Kunwar et al., 2015) support the idea that discrete hypothalamic 563 nuclei are sufficient for generating underlying emotional states concurrent with behavioral 564 output. Given that subsets of PVH neurons drive the autonomic and neuroendocrine 565 components of stress, the possibility of PVH neuron collaterals to brain sites that promote associated behaviors is becoming increasingly clear (Fuzesi et al., 2016). Stress alters 566 defensive expression (Mongeau et al., 2003; Li et al., 2018); therefore, neural circuits 567 568 responsive to stress may modulate behavioral action based on context and/or experience. 569 Supporting this, our findings show that the $PVH \rightarrow vMB$ circuit drives different defensive behaviors based on the testing environment. One striking finding in this study is that optogenetic 570 stimulation of $PVH \rightarrow vMB$ projections drives aversion learning. This aversion learning may be 571

related to a general function of vMB neurons, as supported by previous studies showing that
distinct vMB circuits have been shown to drive emotional learning processes (Lammel et al.,
2012; Root et al., 2014; Barbano et al., 2016; Nieh et al., 2016; Qi et al., 2016), and alter
behavioral outputs in response to stress (Chaudhury et al., 2013; Tye et al., 2013). To our
knowledge, this is the first study that links the PVH function to behavioral conditioning. Further
studies are required to examine the circuit mechanism underlying the conditioning.

578 The majority of PVH neurons use glutamate as a neurotransmitter (Xu et al., 2013). 579 Consistently, our results suggest that glutamatergic transmission from PVH onto vMB neurons was required for defensive behaviors, and contributed significantly to the evoked self-grooming 580 581 behavior. Interestingly, glutamate release from PVH neurons was not absolutely required for the evoked grooming response, suggesting non-glutamatergic, likely neuropeptidergic action, which 582 is in stark contrast to an absolute requirement for glutamate release from lateral hypothalamic 583 neurons in promoting self-grooming behaviors (Mangieri et al., 2018). Of note, less time spent 584 on grooming by photostimulation of Sim1-Cre::ChR2^{PVH->vMB} mice, compare to KOs, is likely due 585 to the competing time spent in jumping behavior, which is supported by increased grooming 586 587 post-stimulation when no jumping was observed. Delayed postsynaptic responses inherent to neuropeptide signaling (van den Pol, 2012) may indeed explain the persistence in grooming 588 589 following light cessation, as well as the delayed initiation of grooming following light stimulation 590 of PVH in the absence of glutamate release. Provided that activation of corticotropin-releasing 591 hormone (CRH) cells in PVH promotes grooming (Fuzesi et al., 2016), and that VTA neurons 592 expressing CRH receptors play a role in stress-induced alterations in behavior (Holly et al., 593 2016), it is possible that CRH signaling from PVH onto midbrain neurons drives the evoked 594 grooming behavior observed here. Nevertheless, future investigation will be needed to identify the specific neuropeptide populations involved. 595

596 Despite extensive research on the impact on behavior via changes in vMB neuron 597 activity, specific upstream sites for glutamatergic transmission onto midbrain glutamate neurons 598 remain largely unexplored (Morales and Margolis, 2017). Here, we identified the PVH as a 599 source of glutamatergic input onto midbrain neurons in driving defensive behaviors. Given the previous findings on vMB glutamatergic neurons in aversion (Root et al., 2014; Qi et al., 2016), 600 we explored the contribution of these neurons. Glutamatergic neurons are part of downstream 601 602 neurons that drive escape behaviors, as evidenced from reduced jumping and time duration in 603 hut with silencing vMB glutamatergic neurons. However, glutamatergic neural silencing failed to 604 reduce time spent in grooming or completely suppress light-evoked escape behaviors. One of 605 underlying reasons may be due to inherent caveats of less than one hundred percent

606 transfection with hM4D-Gi via viral targeting; thus, incomplete silencing of glutamatergic 607 neurons may have insufficiently precluded escape responses. Alternatively, given the relatively 608 mild effect on behaviors by silencing glutamatergic neurons, it is most likely that non-609 glutamatergic midbrain neurons also contribute significantly to mediating the behavioral output of the PVH projection. Notably, GABA-releasing VTA neurons are a good candidate for future 610 611 interrogation, as they have been shown to respond to aversive stimuli (Tan et al., 2012) and drive aversion processes (Tan et al., 2012; van Zessen et al., 2012). In addition, although our 612 613 data suggests that only a small number of dopamine neurons are activated by PVH inputs, given their known role in behavior, it is possible dopamine cells may also contribute to aversive 614 615 properties (Lammel et al., 2012) and increased locomotion (Boekhoudt et al., 2016) in response 616 to PVH neuron activation.

The PVH projects to several brainstem regions, some of which have been implicated in 617 various defensive behaviors. For example, the periaqueductal gray (PAG) has been shown to 618 619 participate in freezing, flight, and avoidance behaviors (Deng et al., 2016; Tovote et al., 2016). 620 Recently, a specific neural subset in the parabrachial nucleus (PBN), a major relay for sensory 621 information, was implicated in defensive expression following recall of fearful memories (Campos et al., 2018). Both PAG and PBN are known downstream sites for the PVH in feeding 622 623 regulation (Stachniak et al., 2014; Garfield et al., 2015). Since the PVH to vMB projection promotes defensive behaviors, it is conceivable that PVH projections to the PAG and PBN may 624 625 also exert a similar function. Notably, given an incomplete reversal in behavioral phenotypes by either vMB glutamate receptor antagonism or inhibition of midbrain glutamatergic neurons, it is 626 627 possible that PVH-collateral fiber activation, due to back propagation, may have resulted in 628 activation of PAG and/or PBN. Ultimately, this may lead to redundant manifestation of the observed residual defensive behaviors. This possibility is supported by the similar effect on 629 suppressing feeding by PVH projections to vMB (this study), PAG and PBN (Stachniak et al., 630 631 2014; Garfield et al., 2015). Future functional tracing and behavioral studies will help delineate 632 how distinct PVH projections are coordinated in the generation of defense and feeding in 633 response to changing environments.

Defensive behaviors such as shelter-seeking and escape represent innate behavioral components and are crucial for survival. Maladaptive coping strategies in people, such as social avoidance and behavioral compulsions, may be illustrative of hardwired responses gone awry in a modern world posing an onslaught of novel environmental challenges. Thus, it has become increasingly important to investigate the neural basis of such behaviors, as they can often lead to paralyzing mental disorders such as generalized anxiety (Kashdan et al., 2006).

- eNeuro Accepted Manuscript
- 640 Here, we have uncovered a hypothalamic-vMB pathway that drives and/or promotes
- 641 conditioned aversion and escape, adding to the accumulating picture of how the brain integrates
- and produces emotions and behaviors underlying adaptive, and possibly maladaptive,
- 643 strategies for survival.
- 644
- 645 Author contributions: Study concept and design, L.R.M., Q.T.; Data Acquisition and analysis,
- L.R.M., Y.L., Y.X., R.M.C., Q.T.; Drafting the Manuscript and Figures, Z.J., N.J., Y.X., B.R.A.,
- 647 Q.T.
- 648
- 649
- 650
- 651
- 652
- 653

654 Figure Legends

655	Figure 1. Optogenetic Activation of PVH Neurons Elicits Flight and Escape Behaviors
656	(A) Experimental schematic (left) and ChR2-EYFP expression in Sim1-Cre::Ai9 neurons
657	in PVH (right). III, third ventricle. Scale bar, 300 μm.
658	(B) Whole-cell recordings in PVH-ChR2 neurons responding to 5 Hz-100 ms light
659	pulses.Quantification of time spent grooming in live animals during 5 Hz-100 ms
660	photostimulation of PVH. n = 7-10 animals/group. Two-way repeated measures
661	ANOVA, followed by Dunnett's multiple comparisons test: Interaction F (2, 30) =
662	0.6948, P=0.5070; Genotype F (1, 15) = 1.316, P=0.2692; Light epoch F (2, 30) =
663	12.33, P=0.0001; Subjects (matching) F (15, 30) = 1.699, P=0.1056. Pre-light vs.
664	Light-on, *p<0.05, ***p<0.0005.
665	(C) Time spent grooming before, during, and after 5 Hz-100 ms photostimulation of PVH
666	in Sim1-Cre::GFP ^{PVH} control mice. n = 7 animals. One-way repeated measures
667	ANOVA: Light epoch F (1.619, 9.715) = 0.5018, P=0.5827; Animals F (6, 12) = 2.2,
668	P=0.1155.
669	(D) Latency to initiate grooming following the first pulse of light during a 5 minute PVH-
670	photostimulation session. n = 7 animals/group. Unpaired t-test: t=3.657 df=12. **p =
671	0.0033. Error bars represent SEM.
672	(E) Temporal representation of cumulative grooming bouts, calculated every 10 seconds,
673	during 5 minutes of photostimulation. n = 7 animals/group. Error bars represent SEM.
674	(F) Comparison of total number of grooming bouts between Sim1-Cre and Sim1-
675	Cre::Vglut2 ^{F/F} animals during the 5 minutes of photostimulation. $n = 7$ animals/group.
676	Unpaired t-test: t=2.11 df=12. p = 0.0565. Error bars represent SEM.
677	(G) Number of jumps counted during 5 minutes of PVH photostimulation with 5 Hz-10 ms
678	pulses of light. n = 7-12 animals/group. Two-way repeated measures ANOVA,
679	followed by Dunnett's multiple comparisons test: Interaction F (2, 34) = 1.576,
680	P=0.2215; Genotype F (1, 17) = 1.576, P=0.2263; Light epoch F (2, 34) = 1.576,
681	P=0.2215; Subjects (matching) F (17, 34) = 1, P=0.4813. Pre-light vs. Light-on,
682	*p<0.05.
683	(H) Number of jumps elicited by 5 Hz,100 ms photostimulation of PVH. $n = 7-10$
684 685	animals/group. Two-way repeated measures ANOVA, followed by Dunnett's multiple comparisons test: Interaction F (2, 30) = 5.299, P=0.0107; Genotype F (1, 15) = 5.24,
686	P=0.0370; Light epoch F (2, 30) = 5.299, $P=0.0107$; Subjects (matching) F (15, 30) =
687	1.048, P=0.4392. Pre-light vs. Light-on, ***p<0.0005.

688	(I) Comparison of the number of jumps evoked by 5 minutes of 5 Hz- 10 or 100 ms
689	photostimulation in Sim1-Cre mice. n = 12 animals. Paired t-test: t=2.965 df=11. * p =
690	0.0129. Error bars represent SEM.
691	(J) Correlation between grooming time and number of jumps in Sim1-Cre animals during
692	5 Hz,100 ms PVH photostimulation. $n = 7-10$ animals/group. Pearson Correlation:
693	r ² =0.6056, p=0.0080.
694	(K) Time spent in grooming evoked by 5 minutes of laser stimulation in Sim1-Cre::GFP ^{PVH}
695	control mice (n=7).
696	(L) Number of jumps evoked by 5 minutes of laser stimulation in Sim1-Cre::GFP ^{PVH}
697	control mice (n=7).
698	
699	
700	Figure 2. Effects of Optogenetic Activation of PVH Neurons on Locomotion and Place
701	Preference
702	Behavior observations were made following optogenetic stimulation of PVH Sim1 neurons.
703	(A) Representative locomotion traces before, during, and after 5 Hz,10 ms photostimulation
704	of PVH.
705	(B) Quantification of distance travelled during locomotion test (F). n = 4 animals/group. Two-
706	way repeated measures ANOVA, followed by Dunnett's multiple comparisons test:
707	Interaction F (2, 12) = 12.18, P=0.0013; Genotype F (1, 6) = 16.39, P=0.0067; Light
708	epoch F (2, 12) = 13.47, P=0.0009, Subjects (matching) F (6, 12) = 0.7245, P=0.6385.
709	Pre-light vs. Light-on, ***p<0.0005.
710	(C) (H) Average velocity during the locomotion assay in Figures 1F-G. n = 4 animals/group.
711	Two-way repeated measures ANOVA, followed by Dunnett's multiple comparisons test:
712	Interaction F (2, 12) = 12.22, P=0.0013; Genotype F (1, 6) = 17.9, P=0.0055; Light
713	epoch F (2, 12) = 13.46, P=0.0009; Subjects (matching) F (6, 12) = 0.6841, P=0.6664.
714	Pre-light vs. Light-on, ***p<0.0005.
715	(D) Representative heatmaps of time spent in arena location overlaying activity tracks during
716	Real Time Place Preference/Avoidance Assay (RTPP/A), where one side of the
717	chamber was paired with PVH-photostimulation or inhibition.
718	(E) Quantification of percent time spent in light-on zone during RTPP/A. n = 5-9
719	animals/group. One-way ANOVA, followed by Dunnett's multiple comparisons test: F (2,
720	18) = 6.115, P=0.0094. Sim1-Cre::GFP ^{PVH} vs. Sim1-Cre::ChR2 ^{PVH} , **p<0.005. Error bars
721	represent SEM. (A) Time spent grooming before, during, and after 5 Hz,100 ms

	722	photostimulation of PVH in Sim1-Cre::GFP ^{PVH} control mice. n = 7 animals. One-way
	723	repeated measures ANOVA: Light epoch F (1.619, 9.715) = 0.5018, P=0.5827; Animals
	724	F (6, 12) = 2.2, P=0.1155.
	725	(F) Comparison of distance travelled during the Real Time Place Preference/Avoidance
	726	Assay in Figures 1H-I. n = 5-9 animals/group. One-way ANOVA: F (2, 18) = 0.6295,
	727	P=0.5442. Error bars represent SEM.
	728	
ro Accepted Manuscript	729	Figure 3. Glutamatergic Transmission from PVH to Ventral Midbrain Region.
\mathbf{C}	730	(A) Anterograde tracing schematic showing downstream sites targeted by PVH projections.
S	731	(B) Synaptophysin-EGFP expression in PVH neurons. III, third ventricle; PVH,
	732	paraventricular hypothalamus. Scale bar, 300 µm.
2	733	(C) Synaptophysin-EGFP puncta seen in rostral midbrain adjacent to VTA, bregma level -2.8
	734	mm.
(U)	735	(D) Synaptophysin-EGFP puncta observed in regions surrounding VTA in middle portions of
	736	midbrain, bregma level -3.16 mm.
\leq	737	(E) Synaptophysin-EGFP puncta seen in rostral portions in and surrounding the VTA,
	738	bregma level -3.4 fr, fasciculus retroflexus; MM, medial mammillary nucleus; SUM,
	739	supramamillary nucleus; VTA, ventral tegmental area. Scale bar, 200 μm.
U	740	(F) Optogenetic activation schematic of PVH→ventral midbrain (mdbrn) circuit.
t t	741	(G) (D) cFos observed in rostral midbrain region (bregma level -2.92 mm, -3.08 mm and -3.4
Q	742	mm) adjacent to VTA (indicated by TH immunostaining in green) following
U	743	photostimulation of PVH \rightarrow ventral midbrain fibers in ChR2-injected animals (right) vs.
Ú	744	control (GFP-injected) animals (left). fr, fasciculus retroflexus; MM, medial mammillary
Ŭ	745	nucleus; SUM, supramamillary nucleus; Arrows point to cFos, TH positive cells. IPN,
	746	interpeduncular nucleus; ml, medial lemiscus; VTA, ventral tegmental area. Scale bar,
	747	500 μm.
0	748	(H) Quantification of number of neurons showing cFos staining in GFP and ChR2 mice. n =
	749	3 animals/group; 2 matched sections per mouse were used for quantification. Unpaired
	750	t-test: t=4.456 df=4. *p = 0.0112. Error bars represent SEM.
	751	(I) Quantification of cFos-TH neuron overlap in $PVH \rightarrow ventral$ midbrain photostimulated
	752	animals. Number of TH neurons was not significantly different between groups, but
eNeui	753	number of cFos, TH positive neurons in ChR2 mice was significantly higher vs. those
a	754	found in GFP control mice, though overall number of cFos, TH positive neurons was low
	755	relative to total number of TH cells and cFos positive neurons (Figure 2G). n = 3

23

756	animals/group; 2 matched sections per mouse were used for quantification. T-test for
757	#TH neurons: t=0.7382 df=4, p = 0.5013, n.s., not significant. T-test for #cFos, TH
758	neurons: t=6.375 df=4, **p = 0.0031.
759	
760	Figure 4. Glutamatergic Transmission from PVH to Ventral Midbrain Drives Flight and
761	Escape.
762	
763	(A) Time spent grooming in response to 20 Hz-10 ms photostimulation of PVH $ ightarrow$ ventral
764	midbrain (mdbrn) circuit in GFP control mice. n = 5 animals. One-way repeated
765	measures ANOVA: Light epoch F (1.733, 6.931) = 11.2, P=0.0077; Animals F (4, 8)
766	= 3.15, P=0.0784.
767	(B) Time spent grooming before, during, and after PVH $ ightarrow$ ventral midbrain
768	photostimulation. n = 6-7 animals/group. Two-way repeated measures ANOVA,
769	followed by Dunnett's multiple comparisons test: Interaction F (2, 22) = 5.144,
770	P=0.0147; Genotype F (1, 11) = 2.803, P=0.1223; Light epoch F (2, 22) = 16.47,
771	P<0.0001; Subjects (matching) F (11, 22) = 1.375, P=0.2522. Pre-light vs. Light-on,
772	**p<0.005; Pre-light vs. Post-light, **p<0.005, ***p<0.0005.
773	(C) Number of jumps evoked by 20 Hz,10 ms photostimulation in in GFP control mice. n
774	= 5 animals. Mice did not display jumping behavior during any light epoch period.
775	(D) Quantification of number of jumps elicited by PVH \rightarrow ventral midbrain
776	photostimulation. n = 6-7 animals/group. Two-way repeated measures ANOVA,
777	followed by Dunnett's multiple comparisons test: Interaction F (2, 22) = 7.756,
778	P=0.0028; Genotype F (1, 11) = 7.69, P=0.0181; Light epoch F (2, 22) = 7.756,
779	P=0.0028; Subjects (matching) F (11, 22) = 1.018, P=0.4636. Pre-light vs. Light-on,
780	***p<0.0005.
781	(E) Schematic of pharmacological blockade of glutamate receptors in VTA/ventral
782	midbrain area prior to photostimulation in freely moving animals.
783	(F) Number of jumps evoked by PVH \rightarrow ventral midbrain photostimulation following
784	microinjection of vehicle or glutamate receptor antagonists to ventral midbrain. n = 4
785	animals. Paired t-test: t=3.357 df=3. *p = 0.0438.
786	(G) Representative locomotion tracks in response to light activation of PVH→ventral
787	midbrain circuit.
788	(H) Distance travelled during locomotion assay in (K). n = 5-6 animals/group. Two-way
789	repeated measures ANOVA, followed by Dunnett's multiple comparisons test:

790	Interaction F (2, 18) = 7.862, P=0.0035; Genotype F (1, 9) = 5.221, P=0.0482; Light
791	epoch F (2, 18) = 10.31, P=0.0010; Subjects (matching) F (9, 18) = 1.93, P=0.1124.
792	Pre-light vs. Light-on, ***p<0.0005.
793	(I) Representative heatmaps of time spent in each location superimposed over tracks
794	during RTPP/A assay, where one side of chamber was paired with light activation of
795	PVH- → midbrain circuit.
796	(J) Quantification of percent time spent in the light zone during RTPP/A assay. n = 3-4
797	animals/group. One-way ANOVA, followed by Tukey's multiple comparisons test: F (2, 8)
798	= 18.84, P=0.0009. Sim1-Cre::GFP ^{PVH->mdbrn} vs. Sim1-Cre::ChR2 ^{PVH->mdbrn} , **p = 0.0018;
799	Sim1-Cre::ChR2 ^{PVH->mdbrn} vs. Sim1-Cre::Vglut2 ^{flox/flox} ::ChR2 ^{PVH->mdbrn} , **p = 0.0014. Error
800	bars represent SEM.
801	
802	Figure 5. PVH→Ventral Midbrain Activation on Fast-Refeeding and Aversive
803	Conditioning.
804	(A) Schematic of fast-refeeding experiment where food is placed in a corner of the light-
805	paired side of the arena.
806	(B) Representative heatmaps of time spent in arena location superimposed over tracks
807	during fast-refeeding assay. Dashed rectangular area denotes food zone. One side of
808	the chamber was paired with PVH photostimulation.
809	(C) Percent of total testing time spent in Light-on zone during fast-refeeding assay. n = 4
810	animals/group. Unpaired t-test: t=15.17 df=6; ***p<0.0001. Error bars represent SEM.
811	(D) Time spent in food zone during fast-refeeding assay. n = 4 animals/group. Unpaired t-
812	test: t=11.4 df=6; ***p<0.0001. Error bars represent SEM.
813	(E) Amount of food eaten during fast-refeeding assay. n = 4 animals/group. Unpaired t-test:
814	t=2.936 df=6; *p = 0.0261. Error bars represent SEM.
815	(F) Representative heatmaps and activity tracks during fast-refeeding assay, where one
816	side of the chamber containing food was paired with PVH $ ightarrow$ ventral midbrain (mdbrn)
817	photostimulation. Dashed rectangular area denotes food zone.
818	(G) Percent of time spent in light-on zone during fast-refeeding assay for PVH→ventral
819	midbrain photostimulation. n = 5 animals/group. One-way ANOVA, followed by Tukey's
820	multiple comparisons test: F (2, 12) = 57.5, P<0.0001. Sim1-Cre::GFP ^{PVH->mdbrn} vs. Sim1-
821	Cre::ChR2 ^{PVH->mdbm} , ***p <0.0001; Sim1-Cre::ChR2 ^{PVH->mdbrn} vs. Sim1-
822	Cre::Vglut2 ^{flox/flox} ::ChR2 ^{PVH->mdbrn} , ***p <0.0001. Error bars represent SEM.

823	(H) Time spent in food zone during fast-refeeding assay. n = 5 animals/group. One-way
824	ANOVA, followed by Tukey's multiple comparisons test: F (2, 12) = 6.952, P=0.0099.
825	Sim1-Cre::GFP ^{PVH->mdbrn} vs. Sim1-Cre::ChR2 ^{PVH->mdbrn} , *p = 0.0289; Sim1-Cre::ChR2 ^{PVH-}
826	>mdbrn vs. Sim1-Cre::Vglut2 ^{flox/flox} ::ChR2 ^{PVH->mdbrn} , *p = 0.0127. Error bars represent SEM.
827	(I) Amount of food eaten during the same assay. n = 5 animals/group. One-way ANOVA,
828	followed by Tukey's multiple comparisons test: F (2, 12) = 53.19, P<0.0001. Sim1-
829	Cre::GFP ^{PVH->mdbrn} vs. Sim1-Cre::ChR2 ^{PVH->mdbrn} , ***p<0.0001; Sim1-Cre::GFP ^{PVH->mdbrn}
830	vs. Sim1-Cre::Vglut2 ^{flox/flox} ::ChR2 ^{PVH->mdbrn} , ***p = 0.0002; Sim1-Cre::ChR2 ^{PVH->mdbrn} vs.
831	Sim1-Cre::Vglut2 ^{flox/flox} ::ChR2 ^{PVH->mdbrn} , **p = 0.0030. Error bars represent SEM.
832	(J) Schematic timeline showing experimental conditions during days of aversive
833	conditioning and extinction tests. The initially most preferred side of a chamber
834	containing contextual flooring cues was paired with PVH $ ightarrow$ ventral midbrain
835	photostimulation on the subsequent days of conditioning.
836	(K) Preference for light-paired side across conditioning days and extinction. n = 4-5
837	animals/group. Two-way repeated measures ANOVA, followed by Sidak's multiple
838	comparisons test: Interaction F (6, 42) = 3.435, P=0.0075; Genotype F (6, 42) = 5.013,
839	P=0.0006; Days of conditioning F (1, 7) = 23.73, P=0.0018; Subjects (matching) F (7,
840	42) = 3.496, P=0.0048. Sim1-Cre::GFP ^{PVH->mdbrn} vs. Sim1-Cre::ChR2 ^{PVH->mdbrn} : *p<0.05;
841	**p<0.005. Error bars represent SEM.
842	(L) Distance travelled during the conditioning assay for each day. n = 4-5 animals/group.
843	Two-way repeated measures ANOVA: Interaction F (6, 42) = 0.682, P=0.6650;
844	Genotype F (6, 42) = 4.827, P=0.0008; Days of conditioning F (1, 7) = 0.09281,
845	P=0.7695; Subjects (matching) F (7, 42) = 11.58, P<0.0001. Error bars represent SEM.
846	
847	Figure 6. Activation of Glutamatergic Ventral Midbrain Neurons in Escape Behaviors.
848	(A) Schematic showing viral delivery of ChR2-EYFP to PVH and EGFP to the midbrain in
849	Vglut2-ires-Cre mice. Inset shows schematic of horizontal slice recordings in midbrain
850	area.
851	(B) Light-evoked excitatory post-synaptic responses (oEPSCs) in 20/20 GFP+ cells
852	receiving input from PVH. Red traces showing oEPSCs blocked by glutamate receptor
853	blockers, and partial recovery after wash-out of drugs (blue traces). Scale bar: vertical,
854	100 pA, horizontal, 2 milliseconds (ms).
855	(C) Light-evoked oEPSCs are blocked by TTX and recovered with addition of 4-AP in GFP+
856	cells. Scale bar: vertical, 100 pA, horizontal, 2 ms.

857	(D) Light-evoked oEPSCs are blocked by TTX and recovered with addition of 4-AP in GFP-
858	cells. Scale bar: vertical, 50 pA, horizontal, 2 ms.
859	(E) Comparison of averaged oEPSC amplitude in GFP+ and GFP- cells. Unpaired t-test:
860	t=0.9975 df=36. p = 0.3252 . Error bars represent SEM.
861	(F) Experimental schematic for inhibiting midbrain glutamatergic neurons, using hM4D(Gi),
862	concurrently with photostimulation of the PVH $ ightarrow$ ventral midbrain (mdbrn) circuit with
863	ChR2.
864	(G) Brain slice images of Vglut2-ires-Cre mice showing ChR2-EYFP expression in PVH
865	(left), and hM4D(Gi)-mCherry expression in midbrain area (right). Dashed area shows
866	optic fiber implant trace. III, third ventricle; fr, fasciculus retroflexus; MM, medial
867	mammillary nucleus; PVH, paraventricular hypothalamus; SUM, supramamillary nucleus.
868	Scale bar, 300 µm.
869	(H) cFos immunostaining in the midbrain following intraperitoneal (i.p.) injection of saline
870	(top images) vs. CNO (bottom images) prior to $PVH \rightarrow$ ventral midbrain photostimulation
871	in Vglut2-ires-Cre mice expressing inhibitory DREADD (hM4D(Gi)-mCherry) in midbrain
872	at the bregma levels of -2.92mm (left panels), -3.16mm (middle panels) and -3.4mm
873	(right panels). Arrows point to mCherry positive/cFos overlapping cells. Images
874	representative of 2 animals per group. Scale bars, 300 μ m. fr, fasciculus retroflexus;
875	IPN, interpeduncular nucleus; ml, medial lemiscus; MM, medial mammillary nucleus;
876	SUM, supramamillary nucleus.
877	
878	Figure 7. Activation of Glutamatergic Ventral Midbrain Neurons in Escape Behaviors.
879	(A) Time spent grooming before, during, and after photostimulation of PVH $ ightarrow$ ventral
880	midbrain (mdbrn) following i.p. injection of saline or CNO. n = 5 animals. Two-way
881	repeated measures ANOVA, followed by Dunnett's multiple comparisons test: Interaction
882	(Drug X Light epoch) F (2, 8) = 0.3522, P=0.7135; Drug F (1, 4) = 0.2098, P=0.6707;
883	Light epoch F (2, 8) = 13.17, P=0.0029. Pre-light vs. Post-light, **p<0.005.
884	(B) Number of jumps counted during PVH $ ightarrow$ ventral midbrain photostimulation tests above,
885	following i.p. injection of saline or CNO. n = 5 animals. Two-way repeated measures
886	ANOVA, followed by Dunnett's and Sidak's multiple comparisons tests: Interaction (Drug
887	X Light epoch) F (2, 8) = 8.412, P=0.0108; Drug F (1, 4) = 8.412, P=0.0441; Light epoch
888	F (2, 8) = 4.288, P=0.0543. Pre-light vs. Light-on: **p<0.005, ***p<0.0005. Saline vs.
889	CNO: Light-on, **p<0.005.

890	(C) Schematic for escape-hut assay. Light-off and light-on epochs alternated for eight
891	minutes.
892	(D) Representative heatmap traces, showing relative time spent in each arena location
893	during the escape-hut assay. The first four minutes of the test is shown.
894	(E) Quantification of the number of times animals visited the escape hut following i.p.
895	injection of saline or CNO. Number of hut visits were summed across four 1-minute light-
896	off periods and four 1-minute light-on periods. n = 5 animals. Two-way repeated
897	measures ANOVA, followed by Sidak's multiple comparisons tests: Interaction (Drug X
898	Light epoch) F (1, 4) = 1.054, P=0.3627; Drug F (1, 4) = 0.9091, P=0.3943; Light epoch
899	F (1, 4) = 19.97, P=0.0111. Off vs. On, *p<0.05.
900	(F) Cumulative duration inside the hut during the escape-hut assay. Time spent inside the
901	hut was summed across four 1-minute light-off and four 1-minute light-on epochs. $n = 5$
902	animals. Two-way repeated measures ANOVA, followed by Dunnett's and Sidak's
903	multiple comparisons tests: Interaction (Drug X Light epoch) F (1, 4) = 13.61, P=0.0210;
904	Drug F (1, 4) = 0.4919, P=0.5217; Light epoch F (1, 4) = 11.49, P=0.0275. Off vs. On,
905	**p<0.005. Saline vs. CNO: On, **p<0.005.
906	
907	Online movie clips
908	Movie S1: Self-grooming behaviors elicited by optogenetic stimulation of PVH neurons in control
909	Sim1-Cre mice;
910	
911	Movie S2: Self-grooming behaviors elicited by optogenetic stimulation of PVH neurons in control
912	Sim1-Cre::Vglut2 ^{F/F} mice;

913

Movie S3: Jumping behaviors elicited by optogenetic stimulation of PVH neurons in control
Sim1-Cre mice;

916

917 References

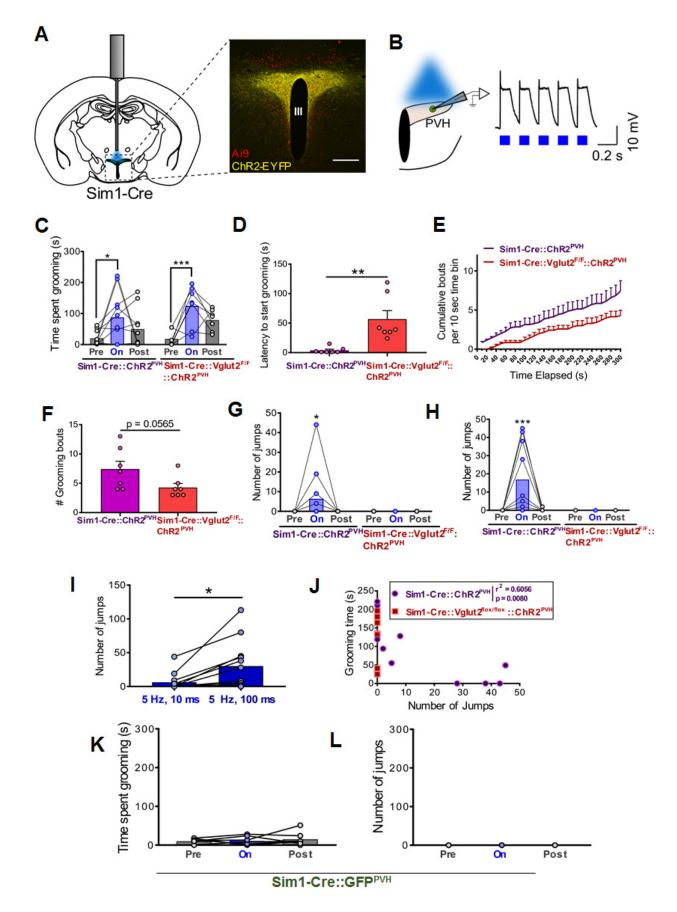
918 Atrens DM, Von V-R (1972) The motivational properties of electrical stimulation of the medial and 919 paraventricular hypothalamic nuclei. Physiology & behavior 9:229-235. 920 Balthasar N, Dalgaard LT, Lee CE, Yu J, Funahashi H, Williams T, Ferreira M, Tang V, McGovern RA, Kenny 921 CD, Christiansen LM, Edelstein E, Choi B, Boss O, Aschkenasi C, Zhang CY, Mountjoy K, Kishi T, 922 Elmquist JK, Lowell BB (2005) Divergence of melanocortin pathways in the control of food intake 923 and energy expenditure. Cell 123:493-505. 924 Barbano MF, Wang HL, Morales M, Wise RA (2016) Feeding and Reward Are Differentially Induced by 925 Activating GABAergic Lateral Hypothalamic Projections to VTA. The Journal of neuroscience : the 926 official journal of the Society for Neuroscience 36:2975-2985. 927 Berndt A, Lee SY, Wietek J, Ramakrishnan C, Steinberg EE, Rashid AJ, Kim H, Park S, Santoro A, Frankland 928 PW, Iyer SM, Pak S, Ahrlund-Richter S, Delp SL, Malenka RC, Josselyn SA, Carlen M, Hegemann P, 929 Deisseroth K (2016) Structural foundations of optogenetics: Determinants of channelrhodopsin 930 ion selectivity. Proceedings of the National Academy of Sciences of the United States of America 931 113:822-829. Blanchard DC, Blanchard RJ (2008) Chapter 2.4 Defensive behaviors, fear, and anxiety. In: Handbook of 932 933 Behavioral Neuroscience (Blanchard RJ, Blanchard DC, Griebel G, Nutt D, eds), pp 63-79: 934 Elsevier. Boekhoudt L, Omrani A, Luijendijk MC, Wolterink-Donselaar IG, Wijbrans EC, van der Plasse G, Adan RA 935 936 (2016) Chemogenetic activation of dopamine neurons in the ventral tegmental area, but not 937 substantia nigra, induces hyperactivity in rats. European neuropsychopharmacology : the journal 938 of the European College of Neuropsychopharmacology 26:1784-1793. 939 Campos CA, Bowen AJ, Roman CW, Palmiter RD (2018) Encoding of danger by parabrachial CGRP 940 neurons. Nature 555:617-622. 941 Canteras NS (2008) Chapter 3.2 Neural systems activated in response to predators and partial predator 942 stimuli. In: Handbook of Behavioral Neuroscience (Blanchard RJ, Blanchard DC, Griebel G, Nutt 943 D, eds), pp 125-140: Elsevier. 944 Chaudhury D et al. (2013) Rapid regulation of depression-related behaviours by control of midbrain 945 dopamine neurons. Nature 493:532-536. Deng H, Xiao X, Wang Z (2016) Periaqueductal Gray Neuronal Activities Underlie Different Aspects of 946 947 Defensive Behaviors. The Journal of neuroscience : the official journal of the Society for 948 Neuroscience 36:7580-7588. 949 Ferguson AV, Latchford KJ, Samson WK (2008) The paraventricular nucleus of the hypothalamus - a 950 potential target for integrative treatment of autonomic dysfunction. Expert opinion on 951 therapeutic targets 12:717-727. 952 Fuzesi T, Daviu N, Wamsteeker Cusulin JI, Bonin RP, Bains JS (2016) Hypothalamic CRH neurons 953 orchestrate complex behaviours after stress. Nature communications 7:11937. 954 Garfield AS, Li C, Madara JC, Shah BP, Webber E, Steger JS, Campbell JN, Gavrilova O, Lee CE, Olson DP, 955 Elmquist JK, Tannous BA, Krashes MJ, Lowell BB (2015) A neural basis for melanocortin-4 956 receptor-regulated appetite. Nature neuroscience 18:863-871. 957 Geerling JC, Shin JW, Chimenti PC, Loewy AD (2010) Paraventricular hypothalamic nucleus: axonal 958 projections to the brainstem. The Journal of comparative neurology 518:1460-1499. 959 Herman AM, Ortiz-Guzman J, Kochukov M, Herman I, Quast KB, Patel JM, Tepe B, Carlson JC, Ung K, 960 Selever J, Tong Q, Arenkiel BR (2016) A cholinergic basal forebrain feeding circuit modulates 961 appetite suppression. Nature 538:253-256. Holly EN, Boyson CO, Montagud-Romero S, Stein DJ, Gobrogge KL, DeBold JF, Miczek KA (2016) Episodic 962 963 Social Stress-Escalated Cocaine Self-Administration: Role of Phasic and Tonic Corticotropin

964	Releasing Factor in the Anterior and Posterior Ventral Tegmental Area. The Journal of
965	neuroscience : the official journal of the Society for Neuroscience 36:4093-4105.
966	Hung LW, Neuner S, Polepalli JS, Beier KT, Wright M, Walsh JJ, Lewis EM, Luo L, Deisseroth K, Dolen G,
967	Malenka RC (2017) Gating of social reward by oxytocin in the ventral tegmental area. Science
968	357:1406-1411.
969	Jennings JH, Rizzi G, Stamatakis AM, Ung RL, Stuber GD (2013a) The inhibitory circuit architecture of the
970	lateral hypothalamus orchestrates feeding. Science 341:1517-1521.
971	Jennings JH, Sparta DR, Stamatakis AM, Ung RL, Pleil KE, Kash TL, Stuber GD (2013b) Distinct extended
972	amygdala circuits for divergent motivational states. Nature 496:224-228.
973	Kashdan TB, Barrios V, Forsyth JP, Steger MF (2006) Experiential avoidance as a generalized
974	psychological vulnerability: comparisons with coping and emotion regulation strategies.
975	Behaviour research and therapy 44:1301-1320.
976	Kunwar PS, Zelikowsky M, Remedios R, Cai H, Yilmaz M, Meister M, Anderson DJ (2015) Ventromedial
977	hypothalamic neurons control a defensive emotion state. eLife 4.
978	Lammel S, Lim BK, Ran C, Huang KW, Betley MJ, Tye KM, Deisseroth K, Malenka RC (2012) Input-specific
979	control of reward and aversion in the ventral tegmental area. Nature 491:212-217.
980	Lammers JH, Meelis W, Kruk MR, van der Poel AM (1987) Hypothalamic substrates for brain stimulation-
981	induced grooming, digging and circling in the rat. Brain research 418:1-19.
982	Lammers JH, Kruk MR, Meelis W, van der Poel AM (1988) Hypothalamic substrates for brain stimulation-
983	induced patterns of locomotion and escape jumps in the rat. Brain research 449:294-310.
984 085	Li L, Feng X, Zhou Z, Zhang H, Shi Q, Lei Z, Shen P, Yang Q, Zhao B, Chen S, Li L, Zhang Y, Wen P, Lu Z, Li X,
985 086	Xu F, Wang L (2018) Stress Accelerates Defensive Responses to Looming in Mice and Involves a
986 987	Locus Coeruleus-Superior Colliculus Projection. Current biology : CB 28:859-871.e855. Madisen L, Zwingman TA, Sunkin SM, Oh SW, Zariwala HA, Gu H, Ng LL, Palmiter RD, Hawrylycz MJ,
988	Jones AR, Lein ES, Zeng H (2010) A robust and high-throughput Cre reporting and
989	characterization system for the whole mouse brain. Nature neuroscience 13:133-140.
990	Mangieri LR, Lu Y, Xu Y, Cassidy RM, Xu Y, Arenkiel BR, Tong Q (2018) A neural basis for antagonistic
991	control of feeding and compulsive behaviors. Nat Commun 9:52.
992	Mongeau R, Miller GA, Chiang E, Anderson DJ (2003) Neural correlates of competing fear behaviors
993	evoked by an innately aversive stimulus. The Journal of neuroscience : the official journal of the
994	Society for Neuroscience 23:3855-3868.
995	Morales M, Margolis EB (2017) Ventral tegmental area: cellular heterogeneity, connectivity and
996	behaviour. Nature reviews Neuroscience 18:73-85.
997	Nieh EH, Vander Weele CM, Matthews GA, Presbrey KN, Wichmann R, Leppla CA, Izadmehr EM, Tye KM
998	(2016) Inhibitory Input from the Lateral Hypothalamus to the Ventral Tegmental Area Disinhibits
999	Dopamine Neurons and Promotes Behavioral Activation. Neuron 90:1286-1298.
1000	Qi J, Zhang S, Wang HL, Barker DJ, Miranda-Barrientos J, Morales M (2016) VTA glutamatergic inputs to
1001	nucleus accumbens drive aversion by acting on GABAergic interneurons. Nature neuroscience
1002	19:725-733.
1003	Root DH, Estrin DJ, Morales M (2018) Aversion or Salience Signaling by Ventral Tegmental Area
1004	Glutamate Neurons. iScience 2:51-62.
1005	Root DH, Mejias-Aponte CA, Qi J, Morales M (2014) Role of glutamatergic projections from ventral
1006	tegmental area to lateral habenula in aversive conditioning. The Journal of neuroscience : the
1007	official journal of the Society for Neuroscience 34:13906-13910.
1008	Silva BA, Gross CT, Graff J (2016a) The neural circuits of innate fear: detection, integration, action, and
1009	memorization. Learning & memory (Cold Spring Harbor, NY) 23:544-555.

- 1010 Silva BA, Mattucci C, Krzywkowski P, Cuozzo R, Carbonari L, Gross CT (2016b) The ventromedial hypothalamus mediates predator fear memory. The European journal of neuroscience 43:1431-1439. Stachniak TJ, Ghosh A, Sternson SM (2014) Chemogenetic synaptic silencing of neural circuits localizes a hypothalamus-->midbrain pathway for feeding behavior. Neuron 82:797-808. Steimer T (2002) The biology of fear- and anxiety-related behaviors. Dialogues in clinical neuroscience 4:231-249. Sternson SM (2013) Hypothalamic survival circuits: blueprints for purposive behaviors. Neuron 77:810-824. Sutton AK, Myers MG, Jr., Olson DP (2016) The Role of PVH Circuits in Leptin Action and Energy Balance. Annual review of physiology 78:207-221. Tan KR, Yvon C, Turiault M, Mirzabekov JJ, Doehner J, Labouebe G, Deisseroth K, Tye KM, Luscher C (2012) GABA neurons of the VTA drive conditioned place aversion. Neuron 73:1173-1183. Tovote P, Esposito MS, Botta P, Chaudun F, Fadok JP, Markovic M, Wolff SB, Ramakrishnan C, Fenno L, Deisseroth K, Herry C, Arber S, Luthi A (2016) Midbrain circuits for defensive behaviour. Nature 534:206-212. Tye KM, Mirzabekov JJ, Warden MR, Ferenczi EA, Tsai HC, Finkelstein J, Kim SY, Adhikari A, Thompson KR, Andalman AS, Gunaydin LA, Witten IB, Deisseroth K (2013) Dopamine neurons modulate neural encoding and expression of depression-related behaviour. Nature 493:537-541. Vale R, Evans DA, Branco T (2017) Rapid Spatial Learning Controls Instinctive Defensive Behavior in Mice. Current biology : CB 27:1342-1349. van den Pol AN (2012) Neuropeptide transmission in brain circuits. Neuron 76:98-115. van Zessen R, Phillips JL, Budygin EA, Stuber GD (2012) Activation of VTA GABA neurons disrupts reward consumption. Neuron 73:1184-1194.
 - Vong L, Ye C, Yang Z, Choi B, Chua S, Jr., Lowell BB (2011) Leptin action on GABAergic neurons prevents obesity and reduces inhibitory tone to POMC neurons. Neuron 71:142-154.
 - Wang L, Chen IZ, Lin D (2015) Collateral pathways from the ventromedial hypothalamus mediate defensive behaviors. Neuron 85:1344-1358.
 - Watabe-Uchida M, Zhu L, Ogawa SK, Vamanrao A, Uchida N (2012) Whole-brain mapping of direct inputs to midbrain dopamine neurons. Neuron 74:858-873.
 - Xu Y, Wu Z, Sun H, Zhu Y, Kim ER, Lowell BB, Arenkiel BR, Xu Y, Tong Q (2013) Glutamate mediates the function of melanocortin receptor 4 on Sim1 neurons in body weight regulation. Cell Metab 18:860-870.

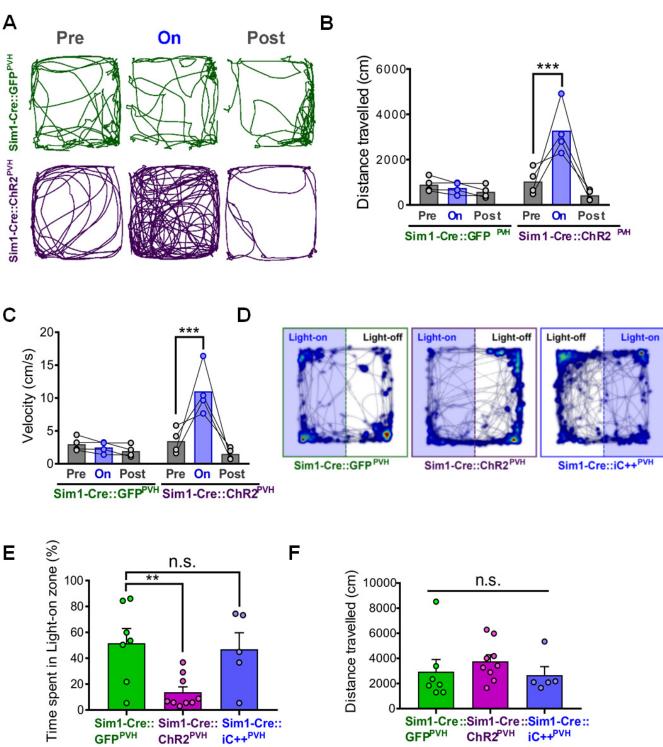
1043

1044



eNeuro Accepted Manuscript

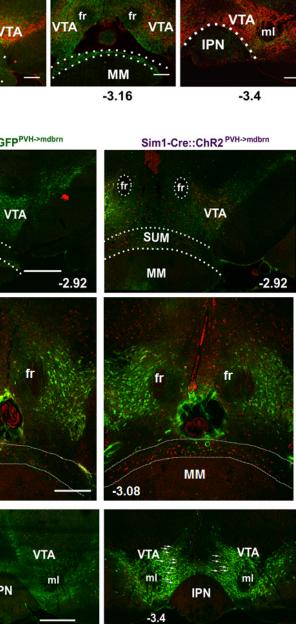
eNeuro Accepted Manuscript



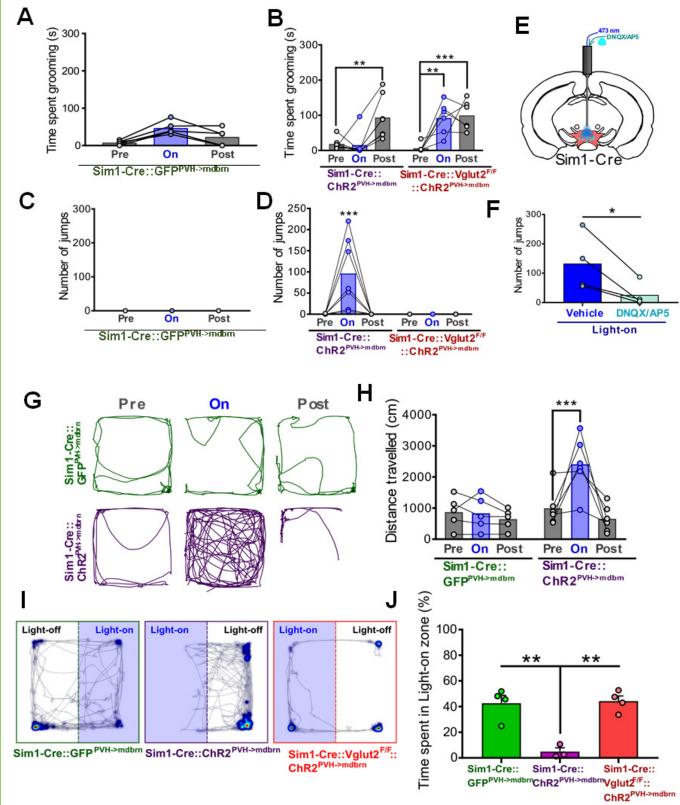
Sim1-Cre:: Sim1-Cre:: ChR2^{PVH} iC++^{PVH}

Ε

Α С в D EF 1a WPRE-pA Syn::EGFP Syn::EGFP Syn::EGFP fr PVH eNeuro Accepted Manuscript Ш VTA SUM ••• MM Sim1-Cre -2.8 G F Sim1-Cre::GFPPVH->mdbrn IH fr fr VTA SUM MM Sim1-Cre Н * 400 Т 300 + ³⁰⁰ 200 # 100 fr fr 100-0 Sim1-Cre:: Sim1-Cre:: GFP^{PVH->mdbm} ChR2^{PVH->mdbm} n.s. MM 1000 -3.08 # Cells 500 VTA VTA 1.7±1.2 30.3±4.3 ml ml 0 IPN ΤН cFos, TH Sim1-Cre::GFP^{PVH->mdbm} -3.4 Sim 1-Cre::ChR2^{PVH->mdbm}

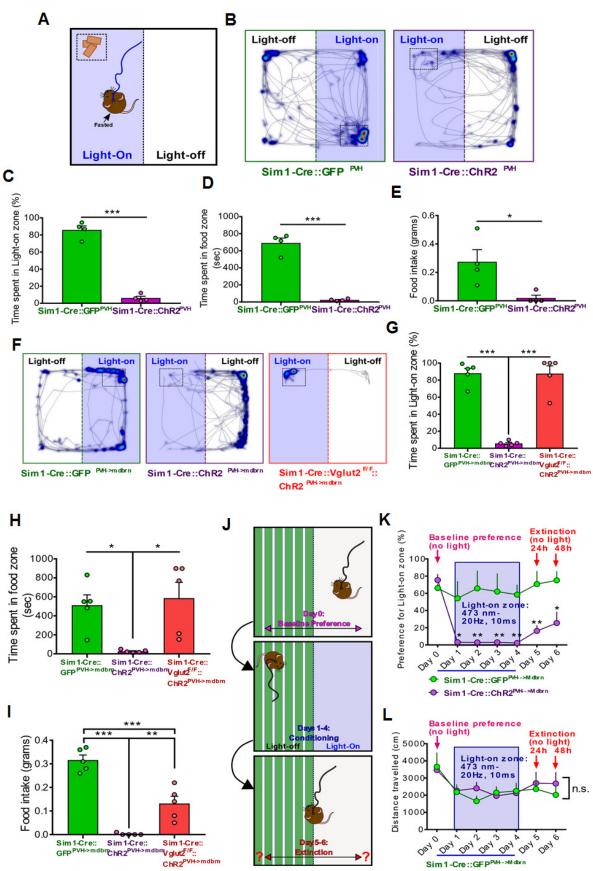


Ε

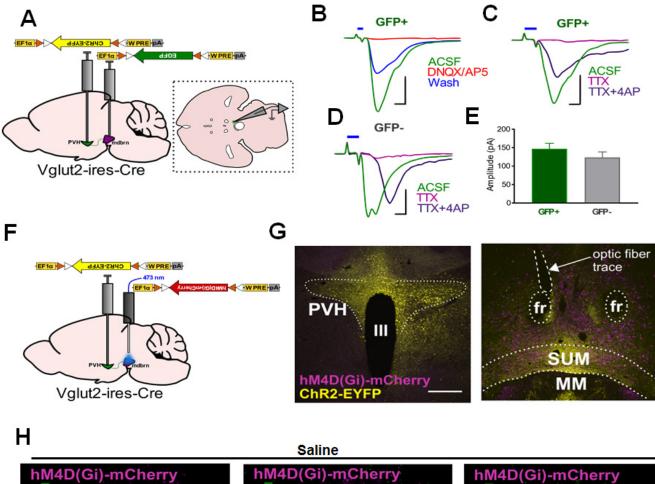


eNeuro Accepted Manuscript

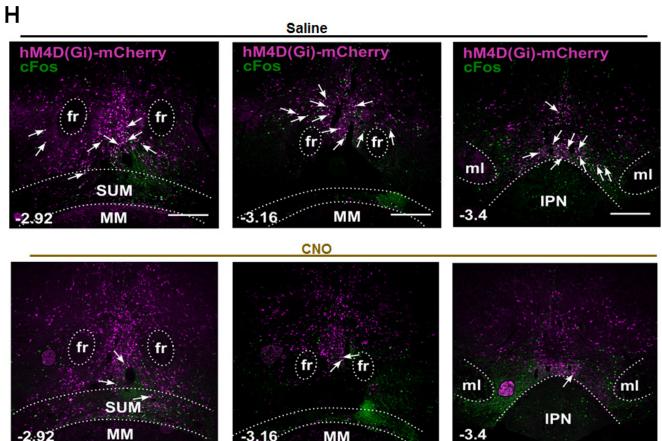
CIRZ



Sim 1-Cre :: Ch R2^{PM+->M dbrn}

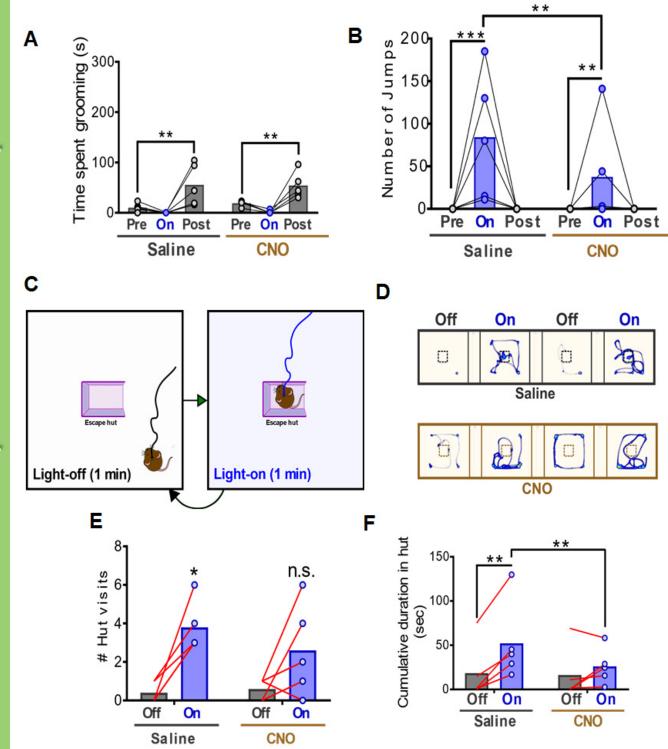


-2.92



MM

-3.16



eNeuro Accepted Manuscript